

Modeling Far-field Acoustical Nonlinearity from F-35 Aircraft during Ground Run-up

Brent Reichman¹

Brigham Young University, Provo, UT, 84602

Alan T. Wall²

Air Force Research Laboratory, Wright-Patterson Air Force Base, OH, 45433

Kent L. Gee³ and Tracianne B. Neilsen⁴

Brigham Young University, Provo, UT, 84602

J. Micah Downing⁵ and Michael M. James⁶

Blue Ridge Research and Consulting, LLC, Asheville, NC, 28801

and

Richard L. McKinley⁷

Air Force Research Laboratory, Wright-Patterson Air Force Base, OH, 45433

The high noise levels associated with full-scale military aircraft result in nonlinear propagation, which results in acoustic shock formation and can alter noise perception. This propagation has been modeled for other aircraft but previous studies have been limited in scope, showing results for only select engine conditions and angles. Recent data measured near an F-35B allow for a more complete analysis of nonlinear propagation. Visual inspection of waveforms shows shock formation and persistence out to distances of up to 1220 m. Using an algorithm based on the Burgers equation, modified to include weak shock theory and an empirical correction for meteorological and ground effects, nonlinear and linear predictions are compared to measurements over a broad range of angles at 305 m. These analyses show that nonlinear effects become important in the maximum radiation direction at 75% thrust and increase with engine condition. At high engine powers, evidence of nonlinear propagation is found in the forward direction.

Nomenclature

| | | |
|-------------|---|---|
| $\alpha(f)$ | = | atmospheric absorption coefficient, Np/m |
| ETR | = | engine thrust request |
| f | = | frequency, Hz |
| l_α | = | absorption length, m |
| MARP | = | microphone array reference point |
| OASPL | = | overall sound pressure level, dB re 20 μ Pa |

¹ Ph.D. Candidate, Dept. of Physics and Astronomy, N283 ESC, AIAA Student Member.

² Postdoctoral Fellow, Battlespace Acoustics Branch, 2610 Seventh St., Bldg. 441, Wright-Patterson AFB, OH 45433, AIAA Member.

³ Associate Professor, Dept. of Physics and Astronomy, N283 ESC, AIAA Senior Member.

⁴ Part-Time Assistant Professor, Dept. of Physics and Astronomy, N283 ESC, AIAA Member.

⁵ Chief Scientist, 29 N Market St, Suite 700, AIAA Member.

⁶ Senior Principal Engineer, 29 N Market St, Suite 700, AIAA Member.

⁷ F-35 Performance & Specialty Engineering Acoustics Lead, Battlespace Acoustics Branch, 2610 Seventh St., Bldg. 441, Wright-Patterson AFB, OH 45433.

OTO = one-third octave
 r = distance from MARP, m
SPL = sound pressure level, dB re 20 μ Pa

I. Introduction

The noise from high-performance military jets is a concern for military personnel who work closely with the aircraft, as well as for communities who may be exposed to such noise. In addition to the high noise levels associated with the aircraft, acoustic shocks may pose an additional risk for both annoyance and hearing loss risk. It is necessary to understand the nature and formation of the acoustic shocks to accurately understand and predict their effects in the sound field. The principles that guide the formation and decay of acoustic shock waves are outlined in nonlinear propagation theory.

The high levels associated with military fighter jet noise mean that linear propagation assumptions are no longer valid. Nonlinear effects are easily observed in the steepening of waveforms in the time domain, which results in spectral broadening and a $1/f^2$ high-frequency spectral slope¹ in the power spectral density. These effects have been observed in both laboratory^{2,3} and full-scale⁴⁻⁸ measurements, although the importance of cumulative nonlinear effects in the laboratory scale has been questioned.^{9,10} The nonlinear propagation of noise has been numerically modeled using many algorithms and in many situations, including military aircraft.¹¹⁻¹⁵ Blackstock¹⁶ was one of the first to attempt to predict nonlinear propagation of jet noise, followed by Morfey and Howell.⁸ Predictions of nonlinear behavior have been shown for multiple aircraft, including the F-18,^{17,18} F-22,^{4,5} and F-35.¹⁹ Gee *et al.*⁴ propagated waveforms from an F-22, from a distance of 61 m to 305 m, along the 125° radial, showing significantly higher levels at high frequencies compared with linear predictions, and showing that measurements agreed closely with nonlinear predictions. A follow-on study in 2008⁵ showed similar results, but broader in scope. Two measurement conditions, 90% ETR and afterburner, were shown at 90°, 125°, and 145°, and multiple propagation distances were considered. Gee *et al.* 2012¹⁹ used a slight modification to the nonlinear propagation algorithm and showed variations in nonlinear propagation with differing weather conditions.

In this paper the nonlinear propagation of jet noise is considered for multiple engine conditions and at a greater angular range than previously shown, including in the forward region of the aircraft. A brief overview of the experimental setup is provided, followed by an examination of time waveforms and spectral maps to show the presence of nonlinear steepening and spectral effects. Spectra at specific locations are shown and examined for nonlinear spectral broadening and other measurement effects such as multi-path interference and atmospheric absorption. Finally, spectra from nonlinear and linear predictions are compared with measurements for multiple angles and engine conditions. These confirm previous findings of significant nonlinear effects in the direction of maximum radiation and show that at high engine conditions a small nonlinear transfer of energy is occurring in the forward direction as well, which may cause changes in the perceived noise.

II. Experiment Overview

In September 2013, extensive measurements were conducted of the F-35A and B sound fields in compliance with the ANSI S12.75 standard for the acoustical measurement of installed, high-performance jet engine noise.²⁰ These measurements included data from 19.2 m to 1220 m over a wide range of angles, with multiple recordings of each engine condition for each aircraft. These measurements allow a wide range of analyses to take place, with comparisons between aircraft, weather conditions, angle, and engine power. In this section an overview of the experiment layout is presented, followed by a brief description of key results.

A. Experiment Layout

A detailed description of the ground run-up measurements has been given by James *et al.*²¹, and as such only a short explanation will be given here. As can be seen in Fig. 1, microphones were placed in over 235 locations around the tethered aircraft, with some located in arrays near the shear layer, and many located in arcs located at $r = 19.2, 28.7, 38.1, 76.2, 152,$ and 305 m from a predetermined microphone array reference point (MARP), located roughly 7 m from the engine's nozzle exit. In addition to the various arrays located within 305 m of the MARP, microphones were hung at multiple heights from two cranes located at 610 m and 1220 m from the MARP, along the radial 135° relative to the nose of the plane. Microphones were also located 9.1 m (30 ft) above the ground at 610 m and 1220 m along 120° and 150° radials. Measurements were taken as the tethered aircraft was operated at various engine conditions, from idle to maximum afterburner, for both the A and B variants.



Figure 1. Measurement locations near Pad 18 at Edwards Air Force Base. Various arrays and arcs of microphones were located around the aircraft, including two cranes not pictured at 610 and 1220 m along the 135° radial, which featured microphones 9.14 m above the ground.

B. Waveform Propagation

The sound levels produced by military aircraft are high, such that nonlinear propagation effects are likely to be seen. These propagation effects are often seen in the form of waveform steepening and shock formation, which can be verified by visual inspection of the time waveforms. Time-aligned waveforms measured at maximum afterburner at different distances along the 135° radial are displayed in Fig. 2, similar to those shown by Gee *et al.*⁵ and Fievet *et al.*²² The 135° radial is shown as cranes at $r = 610$ m and 1220 m were located along this radial. The waveforms are normalized by the maximum value at each distance and plotted against retarded time. In the time-aligned waveforms, individual shock waves form and decay as the wave propagates from 19.2 m to 1220 m. For example, the rapid rises in pressure at 0.905 s and at 0.953 s in the waveform at 19.2 m have steepened into shocks by 38.1 m, and these shocks persist past 152 m. In the 305 m waveform, the 0.953 s shock has started to decay, whereas the 0.905 s shock continues to 305 m and begins to decay by 610 m. These waveforms show that nonlinear steepening occurs along the maximum radiation direction as the wave propagates away from the jet, and that acoustic shocks can be seen at least 610 m away from the jet. The formation and decay of shocks from 19.2 m to 1220 m is evidence of cumulative nonlinear propagation.

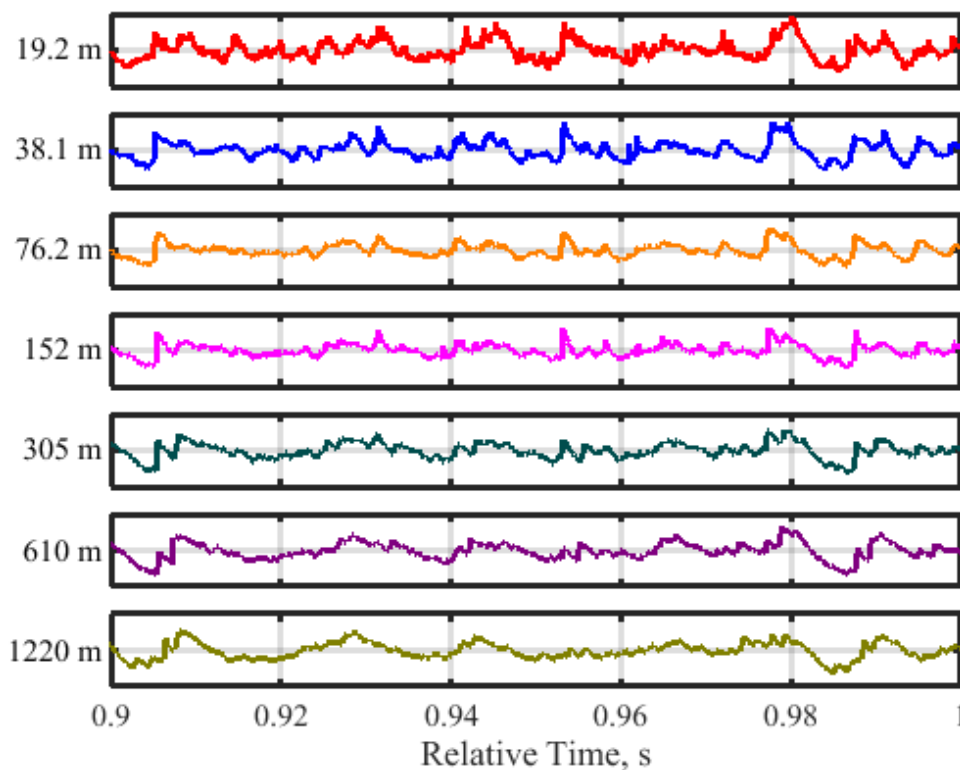


Figure 2. Time-aligned Waveforms along the 135° Radial. Waveforms measured at various distances and plotted against retarded time show the formation and decay of individual shocks.

C. Spectral Maps

A close examination of the angular variation in the OTO spectra is provided at 76.2 m and 305 m in Figs 3-4 for 50%, 75%, 100%, and 130% ETR. The spectra are shown from 0° to 160° and from 50 Hz to 20 kHz. Although the spectra are not shown for the maximum afterburner case, 150% ETR, they are similar to those seen at 130% in Fig. 3(d), with a small increase in level. At $r = 76.2$ m, the far-field directivity of the source is identifiable and shifts farther from the engine nozzle centerline as ETR increases – from 145° at 50% to 120° at 130%. In this region of maximum radiation, the peak frequency is located between 70-300 Hz, though the peak frequency changes slightly with engine condition. Additional effects on the spectra can be seen due to multi-path interference in both figures, in particular at 90° as multiple dips and peaks are seen with increasing frequency.

The nonlinear steepening seen in Fig. 2 is also evident in the frequency domain. As the waveform steepens, the spectrum broadens, with the primary energy transfer to higher frequencies, which can be thought of as a lack of absorption. The average temperature for these measurements was 20.9°C, the relative humidity was 44.0%, and the ambient pressure was 93.4 kPa. For these atmospheric conditions, the linear absorption between 76.2 m and 305 m, calculated according to the ANSI standard,²³ predicts a loss of more than 100 dB at 20 kHz. Thus, in the case of linear propagation, the difference in levels at 20 kHz shown in Figs 3 and 4 would be below the noise floor of the microphones at $r = 305$ m. While the levels above 10 kHz are below the noise floor of 40 dB for the lower engine conditions in Fig. 4(a) and (b), at the higher engine conditions, the 20 kHz levels are greater than 80 dB along the far-field directivity angle (Fig. 4(c) and (d)). The fact that the high-frequency levels are greater than the noise floor of the microphones indicates that nonlinear propagation is still supplying energy to the higher frequencies at 305 m over a large range of angles. A more detailed analysis of spectra at specific microphones can help quantify the nonlinear effects.

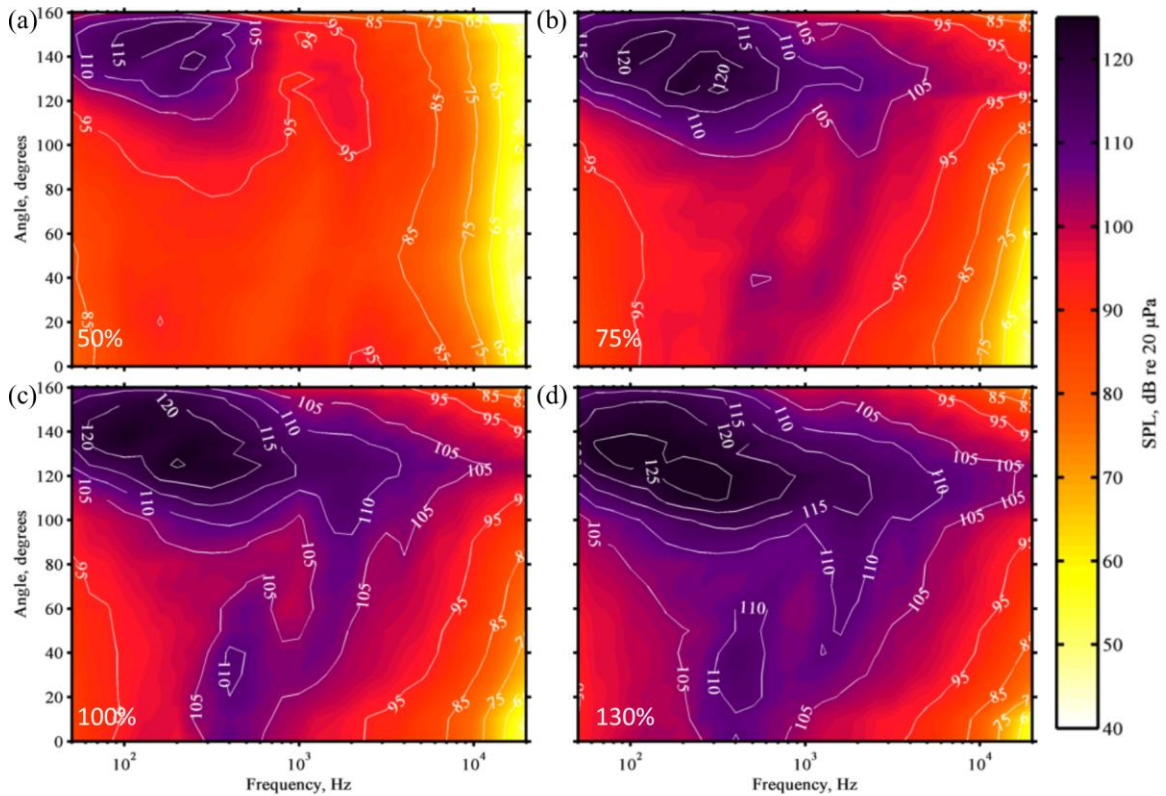


Figure 3. OTO Spectra at $r = 76.2$ m from the MARP. OTO spectra are plotted as a function of angle (relative to the nose of aircraft) for four engine conditions: (a) 50%, (b) 75%, (c) 100%, and (d) 130% ETR.

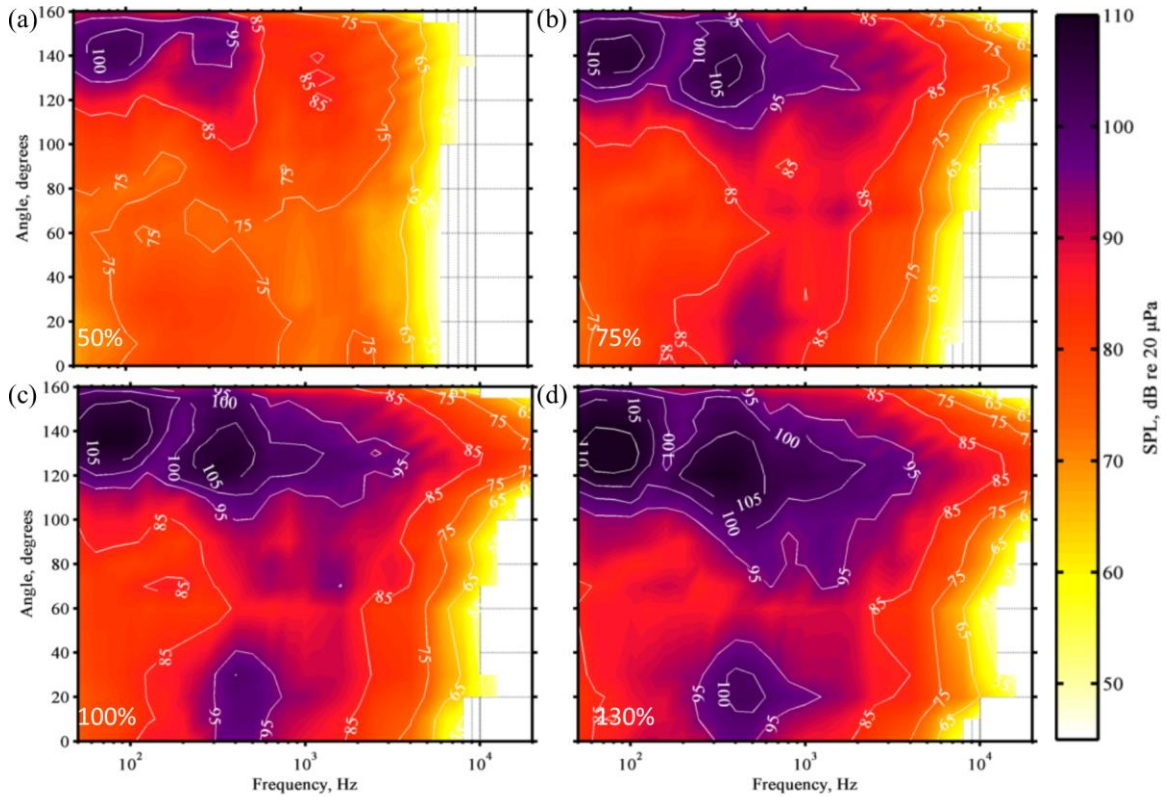


Figure 4. OTO Spectra at $r = 305$ m from the MARP. OTO spectra are plotted as a function of angle (relative to the nose of aircraft) for four engine conditions: (a) 50%, (b) 75%, (c) 100%, and (d) 130% ETR.

III. Spectral Analysis

The waveform steepening and spectral maps shown in the previous section provide evidence for nonlinear propagation effects in the far field of the F-35B. However, a detailed analysis of the spectra at individual distances and angles can shed light on where nonlinear propagation is occurring and to what extent. Before this analysis, linear and nonlinear propagation effects on the spectrum will be discussed, following which the spectra will be shown.

A. Spectral Effects

As described briefly above, waveform steepening results in a transfer of spectral energy from the peak-frequency region to higher frequencies. In a waveform containing weak shocks, the spectrum of the noise decays at $1/f^2$.¹ For OTO spectra, which are presented here, the expected roll-off rate for high frequencies is 10 dB/decade.⁵ As the waveform continues to propagate, rise time increases and the shocks begin to thicken. As the shocks thicken the linear absorption at high frequencies has a large effect and the roll-off of the spectrum at higher frequencies increases. For initially sinusoidal plane waves this occurs when the distance, r , is equal to the absorption length, defined as

$$l_{\alpha} = 1/\alpha(f), \quad (1)$$

where $\alpha(f)$ is the absorption coefficient.²⁴ For sinusoidal plane waves, this distance is independent of initial source amplitude. Others have shown this transition to what is called the old-age region while incorporating geometric spreading²⁵ and for broadband noise.²⁶ When the absorption length is equal to the distance from the noise source, a steeper spectral roll-off can be expected. The distances at which far-field microphones were situated in the current experiment are listed in Table 1 along with the frequency associated with the absorption length at that distance. The absorption length is calculated using meteorological data from the measurements over a range of frequencies, then

the data are interpolated to find the frequency with the absorption length at the microphone distances from the MARP.

Table 1. The frequencies with an absorption length corresponding to measurement locations. The absorption length is calculated using meteorological data from the given measurement time over a range of frequencies, then the data are interpolated to find the frequency with the absorption length at the microphone distances from the MARP.

| | | | | | |
|-----------------|-----|-----|-----|-----|------|
| Distance (m) | 76 | 152 | 305 | 610 | 1220 |
| Frequency (kHz) | 8.0 | 5.5 | 3.8 | 2.4 | 1.5 |

In addition to the nonlinear effects that affect the high-frequency roll-off of the spectra, ground reflections can have a significant effect on discrete frequencies. Both the aircraft nozzle and the microphones used to record data were located off of the ground, producing a minimum of two paths by which sound can travel from the noise source to the microphone, either directly through the air or after reflecting off of the ground. If we assume a point source at a height of 1.82 m above the MARP and a rigid ground, the discrete frequencies at which the two paths will interfere destructively can be found if a finite ground flow resistivity is assumed,²⁷ in this case the value of 3,000 rayls was used, typical of hard-packed earth. Although the model gives the effect of constructive and destructive interference over a range of frequencies, Table 2 lists the first frequency at which destructive interference is observed. This null has the most significant effect on OTO spectra due to averaging, and the effects of higher frequency nulls are diminished due to turbulence in the atmosphere.^{28,29}

Table 2. Microphone heights and expected interference nulls for various distances. The heights of the microphones located in arcs of various radii are listed. These microphone heights are then used with a nozzle height of 1.82 m to calculate the frequency at which an interference null would be expected using a ground flow resistivity of 3,000 rayls.

| | | | | | | |
|-----------------|------|------|------|------|------|------|
| Distance (m) | 19 | 29 | 39 | 76 | 152 | 305 |
| Mic. Height (m) | 1.52 | 1.52 | 1.52 | 3.66 | 5.49 | 9.14 |
| Frequency (kHz) | 0.54 | 0.78 | 0.96 | 0.78 | 0.89 | 0.89 |

B. Spectral Comparisons

With the above analyses and expected behavior concerning spectral decay, absorption length, and ground reflections, the spectra measured at specific locations can be examined for evidence of each of these phenomena. The spatial dependence of the spectra along 30°, 90°, 135°, and 150° radials are shown in Figs. 5-8, respectively. These angles are chosen because they correspond with spatial regions where the noise properties are significantly different: forward direction, sideline of the MARP, near the maximum radiation direction and farthest downstream positions. Though some angles had microphones at a greater range of distances, at all four angles the waveforms measured at 38.1 m, 76.2 m, and 305 m from the MARP are shown for four engine conditions: (a) 50%, (b) 75%, (c) 100%, and (d) 130% ETR.

As the ETR increases, the spectral shape at higher frequencies changes for all four angles. The greatest nonlinear effects are expected in the maximum radiation direction, shown in Fig. 7. In this direction, the levels at higher frequencies are greater than 80 dB at $r = 305$ m from the source, a level inconsistent with linear losses. In addition, from linear assumptions one would expect that between 38 m and 76 m the spectral levels at higher frequencies in Fig. 7(d) to have decreased relative to lower frequencies. Instead, the spectral shape is essentially unchanged, as the nonlinear transfer of energy to higher frequencies balances out the loss due to absorption. This change in the slope of the high-frequency portion of the spectral shape is most easily observed in the spectra at 76 m, but can also be seen in the 152 m and 305 m spectra, indicating nonlinear propagation. If shocks are present in the waveform, the high-frequency roll-off should be roughly 10 dB/decade, and this is seen to some extent for all four ETR shown. The roll-off should also steepen at the frequencies calculated in Section III A. as the distance is on the same order of magnitude for the absorption length of that frequency, and these values do correspond with changes in the spectral shape, especially at greater ETR. These same trends are seen in Figs. 6 and 8, though at a slightly lower level. Also of note is the strong evidence of a ground reflection null for all ETR in Fig. 6. For the spectra at 19 m, this null occurs between 500-600 Hz, precisely at the value calculated in Section III A. Also evident is the presence of interference in the spectra of microphones at 610 and 1220 m at frequencies well below those at which ground

reflections would be expected. These interference nulls provide further evidence for a downward-refracting atmosphere, due to either a gradient in wind or temperature.

Along the 30° radial in Fig. 5(a), the spectrum measured at 76 m begins to sharply roll off at roughly 3 kHz, but in Fig. 5(c) and 5(d) the roll-off is much more gradual, even at frequencies as high as 20 kHz, where absorption should be having a large effect. The persistence of the shallower spectral slope at high frequencies implies that the high-frequency losses expected from atmospheric absorption are being countered by nonlinear propagation effects. Though the rate of roll-off is greater than would be expected if shocks were present, it is still smaller than would be expected if purely linear behavior is assumed. Because of this, the spectral shapes alone do not conclusively exhibit the effects of far field nonlinear propagation in the forward direction. This concept is revisited in a later section.

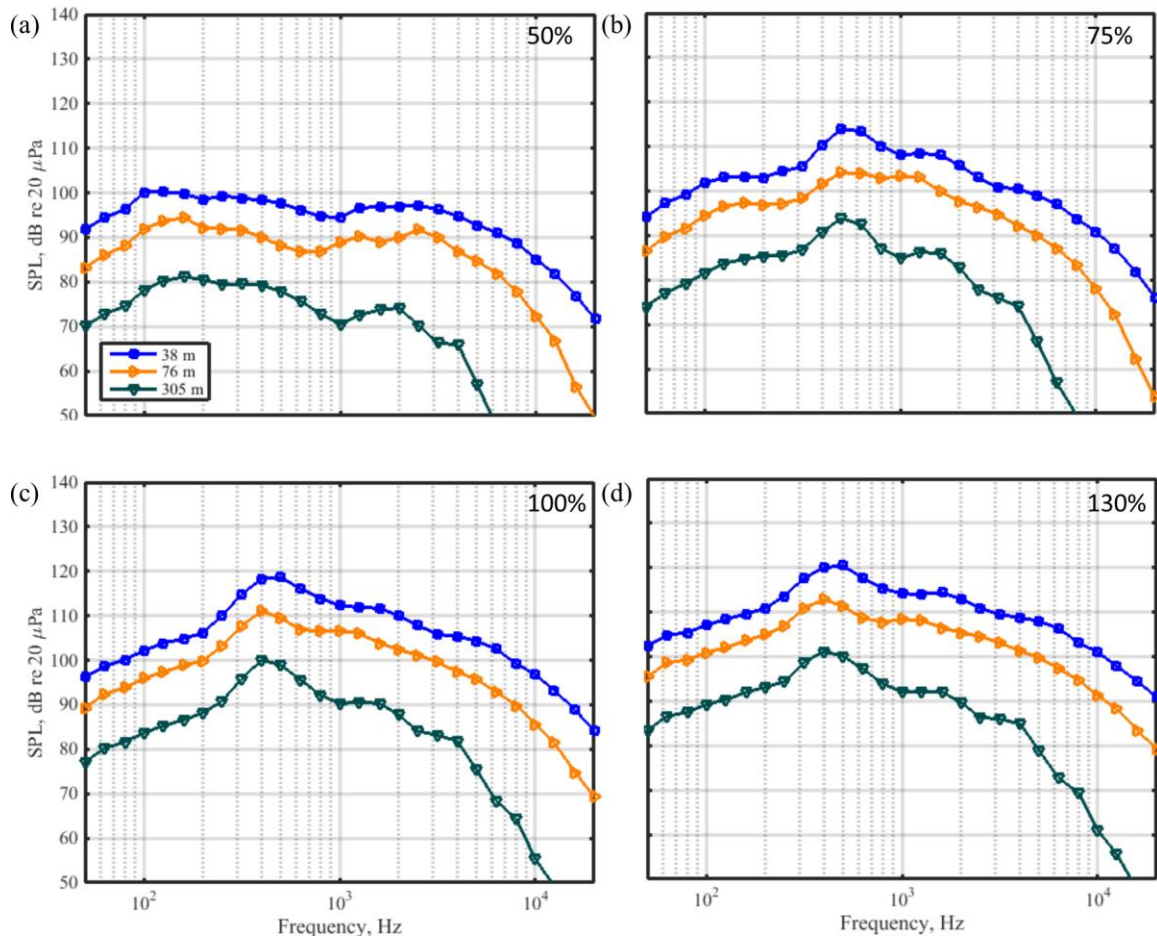


Figure 5. OTO Spectra along the 30° radial as a function of engine condition. The four plots show the OTO spectra calculated at (a) 50% ETR, (b) 75% ETR, (c) 100% ETR, and (d) 130% ETR.

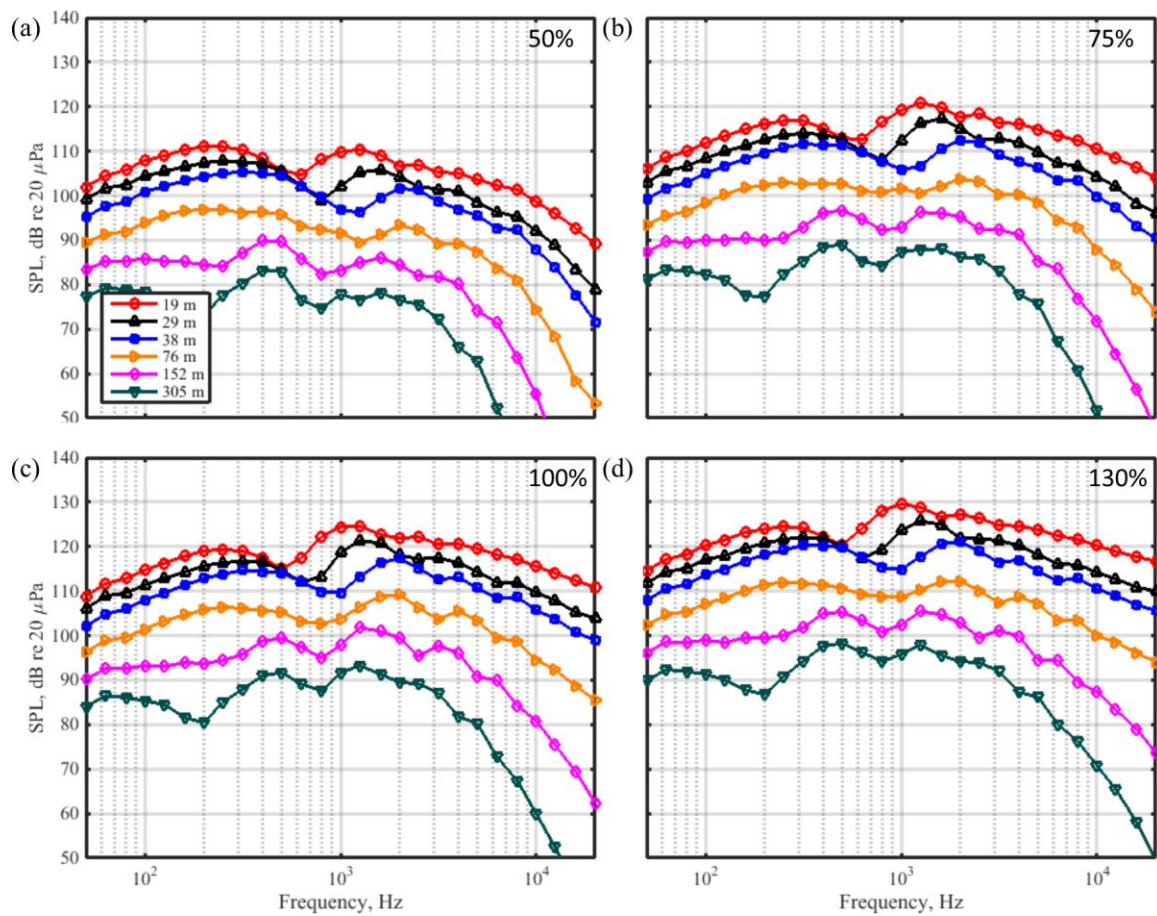


Figure 6. OTO Spectra along the 90° radial as a function of engine condition. The four plots show the OTO spectra calculated at (a) 50% ETR, (b) 75% ETR, (c) 100% ETR, and (d) 130% ETR.

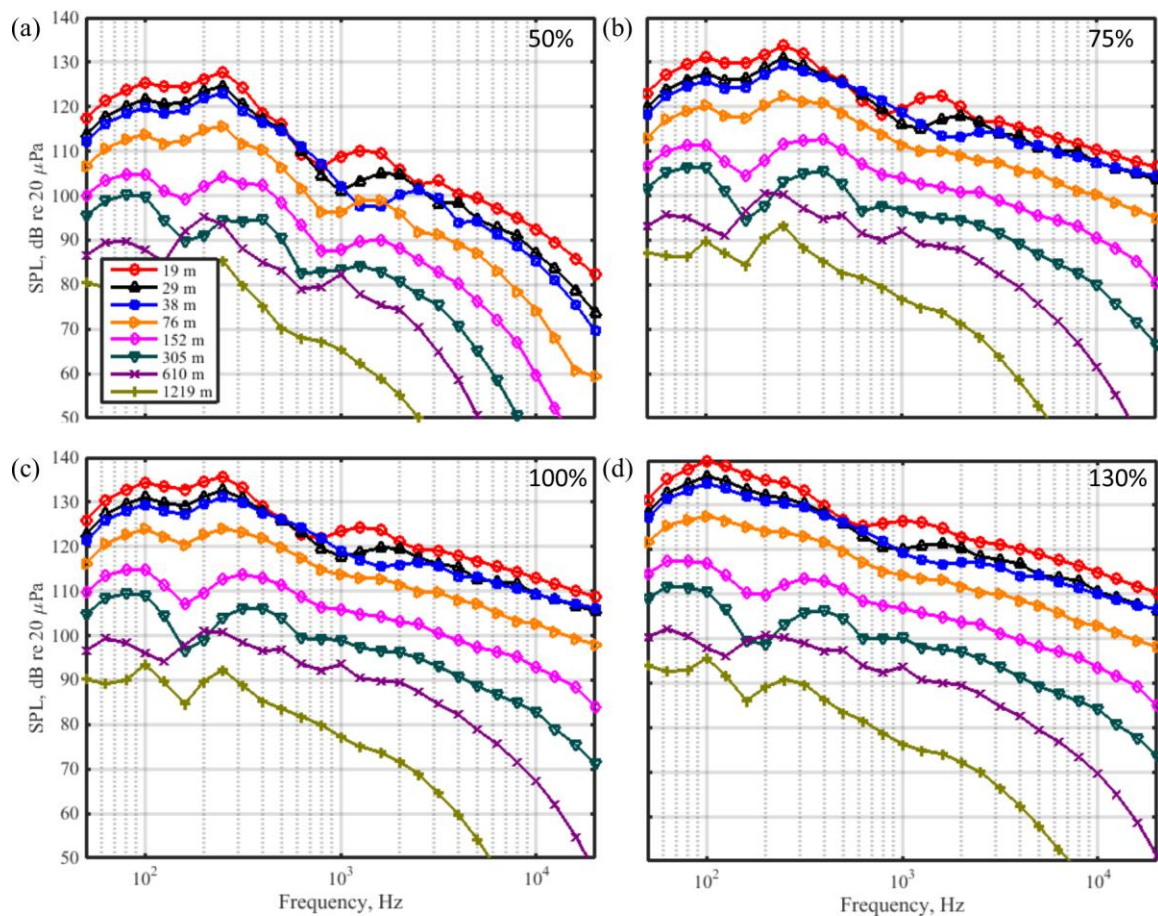


Figure 7. OTO Spectra along the 135° radial as a function of engine condition. The four plots show the OTO spectra calculated at (a) 50% ETR, (b) 75% ETR, (c) 100% ETR, and (d) 130% ETR.

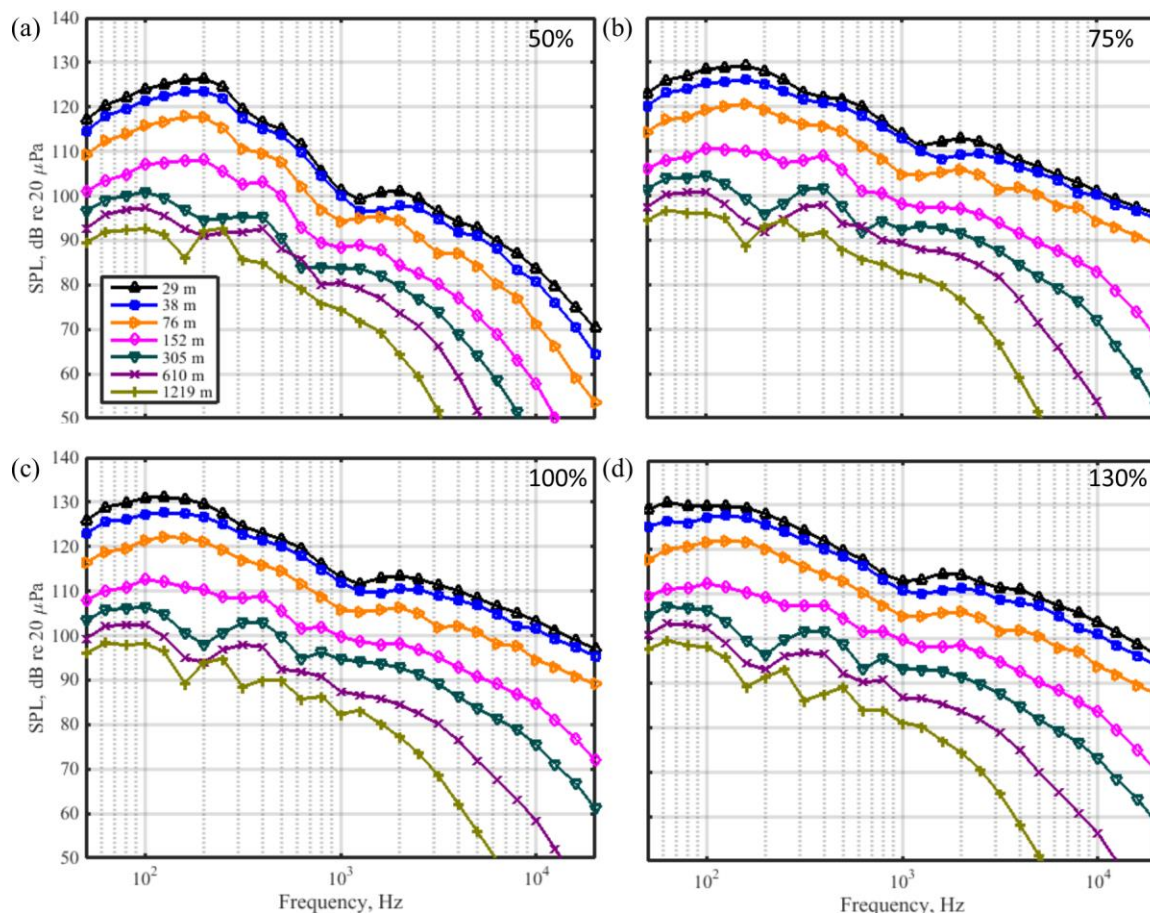


Figure 8. OTO Spectra along the 150° radial as a function of engine condition. The four plots show the OTO spectra calculated at (a) 50% ETR, (b) 75% ETR, (c) 100% ETR, and (d) 130% ETR.

IV. Nonlinear propagation modeling

The above spectra certainly suggest that nonlinear propagation is a factor, at the very least out to 305 m and possibly farther, and at a broad range of angles. However, in order to quantify the effect that nonlinear propagation has on both the waveform and the spectrum, the nonlinear effects must be compared with a linear prediction. To do this, both linear and nonlinear propagation schemes are used to numerically propagate waveforms measured at 76.2 m to 305 m, and the resulting spectra are compared with those calculated from the measured waveform at 305 m. Though three angles have microphones at distances greater than 305 m, this distance is chosen to compare across a wide range of angles from 0° to 160°.

A. Nonlinear algorithm and spectral correction

The nonlinear propagation code is similar to that used by Gee *et al.*¹⁹ It is a hybrid time-frequency domain algorithm based on the Generalized Burgers Equation (GBE) and incorporates geometric spreading, atmospheric absorption, and quadratic nonlinearity as well as weak shock theory developed by Pestorius and Blackstock¹¹ to more efficiently propagate shocks. A similar code that neglects the quadratic nonlinearity is used to propagate the waveforms linearly. The spectra from these nonlinear and linear predictions can be compared against each other and against the spectrum of the measured waveforms.

Multi-path interference presents a problem in comparing numerically propagated waveforms with measurements. Measurements at 76 m have an interference pattern due to the geometry of that location and other weather effects, but these frequency-domain patterns are still carried throughout the propagation process. However, at 305 m an entirely different interference pattern is seen, and the numerical models have no way to correct for these changes. To

account for this difference in spectrum an empirical correction, developed by Gee *et al.* 2007⁴ and used again in Gee *et al.* 2012¹⁹ for meteorological and propagation environment effects not treated by the GBE model, is applied. Based on the assumption that over a short period of time, the changes in spectra due to interference effects and meteorology between the two distances are consistent, the correction is the difference between the spectra from the numerical propagation and the measurement. This correction uses the change in spectrum between the two measurement locations from a low-power measurement where nonlinear effects are minimal, in this case 50% ETR, to correct predictions at higher measurement location. The measured waveform for 50% ETR is nonlinearly propagated to the second location, and the difference between the predicted spectrum and the measured spectrum is calculated. For higher engine power conditions, this difference is then added to the predicted linear and nonlinear spectra, such that

$$SPL_{HP,corr} = SPL_{HP,pred} + (SPL_{LP,meas} - SPL_{LP,pred}) \quad (2)$$

where HP indicates high power, LP low power, $SPL_{HP,corr}$ is the corrected spectrum, and pred and meas refer to the predicted and measured spectra. Note that this correction is only applied below 1 kHz due to noise floor issues at 305 m above this frequency. However, this frequency range corresponds to the largest changes due to interference, and nonlinear propagation effects are small at 50% below 1 kHz.

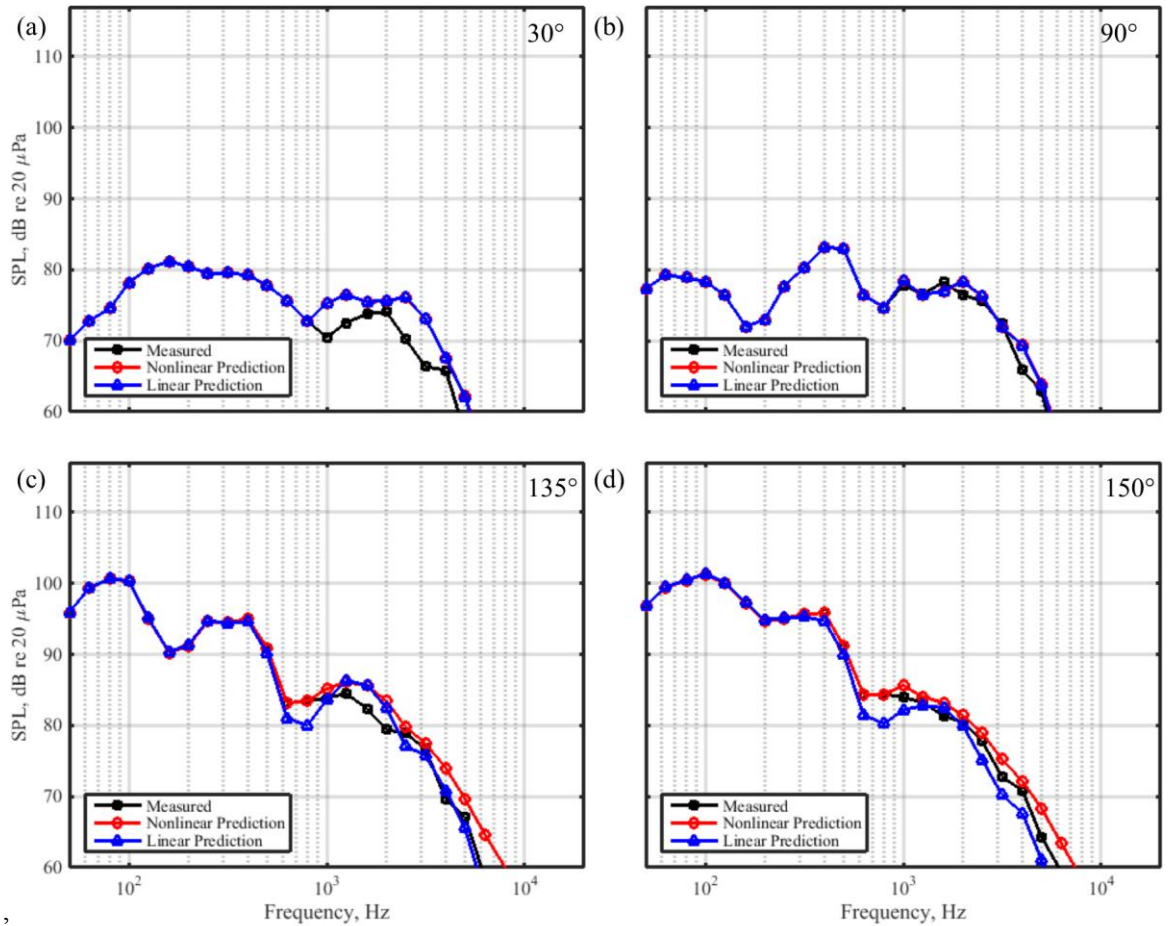
B. Nonlinear prediction comparison

Both the linear and nonlinear propagation algorithms are applied to waveforms measured at $r = 76.2$ m to estimate waveforms at $r = 305$ m. The empirical corrections in Eq. (2) are estimated separately at each angle and applied to the spectra of the numerically propagated waveforms in both the linear and nonlinear cases. The linearly and nonlinearly propagated waveforms are compared with the spectra measured at 305 m for 50% ETR in Fig. 9 at 30°, 90°, 135°, and 150°. For this low ETR, at both 30° and 90° there is essentially no difference between the linear and nonlinear predictions. At 135° and 150° small differences are seen but all three spectra are within a few decibels of each other.

As ETR increases, so do the differences between nonlinear and linear predictions. At 75% ETR, as shown in Fig. 10, nonlinear effects are evident at 135° and 150°, shown in Fig. 10(c) and (d), where there is a large difference among the higher frequencies. In both these cases, the measured spectrum very closely resembles the nonlinear prediction. In spite of differences in the spectra at low frequencies due to interference nulls, the nonlinear propagation code accurately characterizes the high-frequency behavior within 1-2 dB. The difference between the linear and nonlinear predictions is greater at 100% ETR, as shown in Fig. 11. The relative increase in high-frequency energy is again most evident at 135° and 150°, but small differences in the high frequencies can also be seen at 30° and 90° in Fig. 11(a) and 11(b).

In the discussion of Fig. 5 the point is made that the spectral roll-off at high frequencies could show nonlinear behavior in the forward direction. Further evidence is seen in Fig. 11(a) and (b), where nonlinear predictions agree with measured data more closely than linear predictions. The evidence of nonlinear propagation in the forward direction is even clearer at 130% ETR. In Fig. 12(a), the measured spectrum at 8 kHz is 10 dB higher than the linear prediction. Though the nonlinear method slightly overestimates the spectrum at the higher frequencies, it is more accurate than the linear prediction, indicating a degree of nonlinear propagation in the far-field forward direction.

The results show that spectra calculated from measured waveforms closely resemble those using the nonlinear propagation algorithm. In some cases the nonlinear algorithm overpredicts the level at high frequency, but this is possibly due to terrain effects such as dense shrubbery nearby, which could substantially affect higher frequencies. At lower ETR the linear and nonlinear predictions are nearly aligned, but at higher conditions the measured data agrees more closely to the nonlinear predictions, even at 30°, in the forward direction of the aircraft. Because the nonlinear predictions accurately reflect changes in the spectra, in particular at high frequencies, a comparison between linear and nonlinear predictions can be used to quantify the strength of nonlinear effects as a function of angle, which will be shown in the following section.



I can't
Figure 9. OTO spectra at 305 m compared with linear and nonlinear predictions for 50% ETR. Waveforms measured at $r = 76.2$ m are propagated to $r = 305$ m using both linear (blue) and a nonlinear (red) propagation algorithms. The resulting OTO spectra are compared with the spectra at 305 m (black) at (a) 30°, (b) 90°, (c) 135°, and (d) 150°.

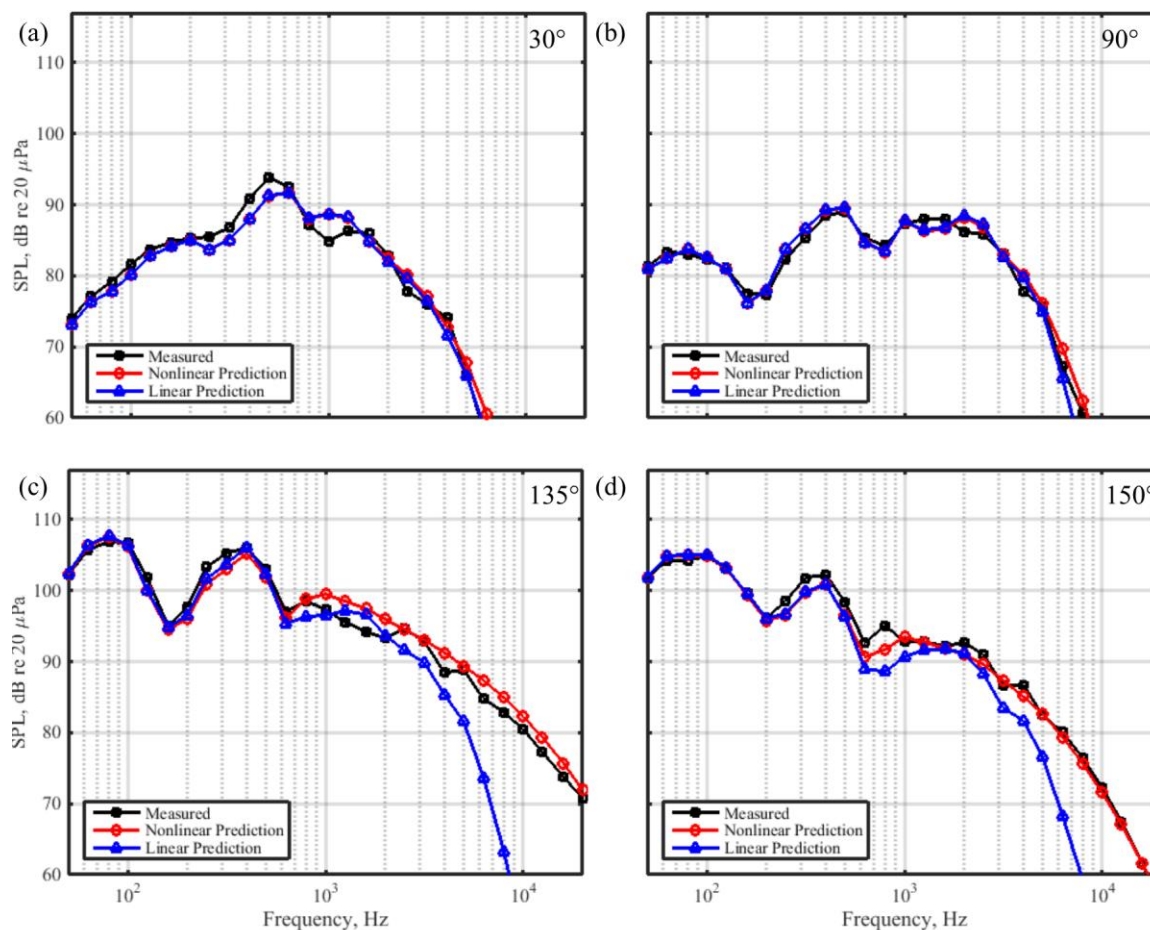


Figure 10. OTO spectra at 305 m compared with linear and nonlinear predictions for 75% ETR. Waveforms measured at $r = 76.2$ m are propagated to $r = 305$ m using both linear (blue) and a nonlinear (red) propagation algorithms. The resulting OTO spectra are compared with the spectra at 305 m (black) at (a) 30°, (b) 90°, (c) 135°, and (d) 150°.

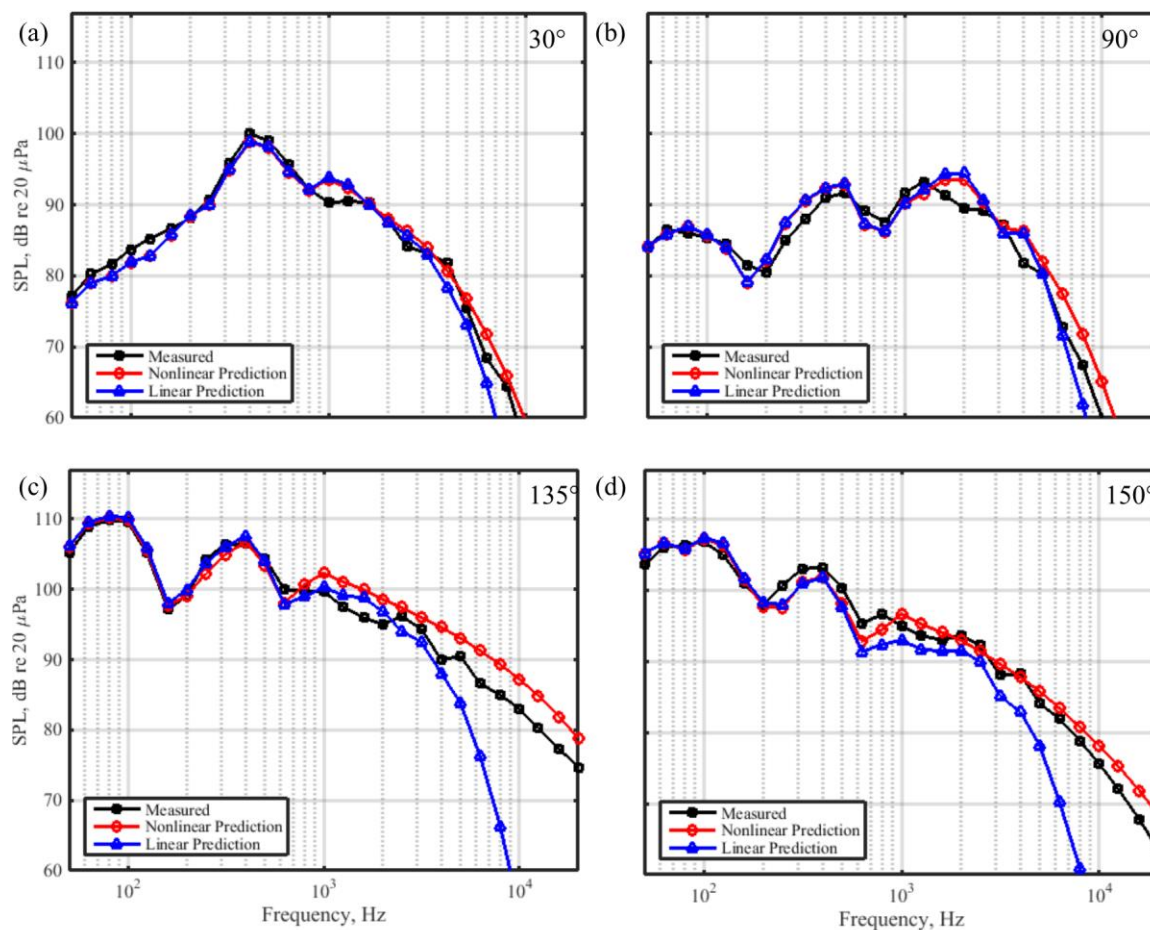


Figure 11. OTO spectra at 305 m compared with linear and nonlinear predictions for 100% ETR. Waveforms measured at $r = 76.2$ m are propagated to $r = 305$ m using both linear (blue) and a nonlinear (red) propagation algorithms. The resulting OTO spectra are compared with the spectra at 305 m (black) at (a) 30°, (b) 90°, (c) 135°, and (d) 150°.

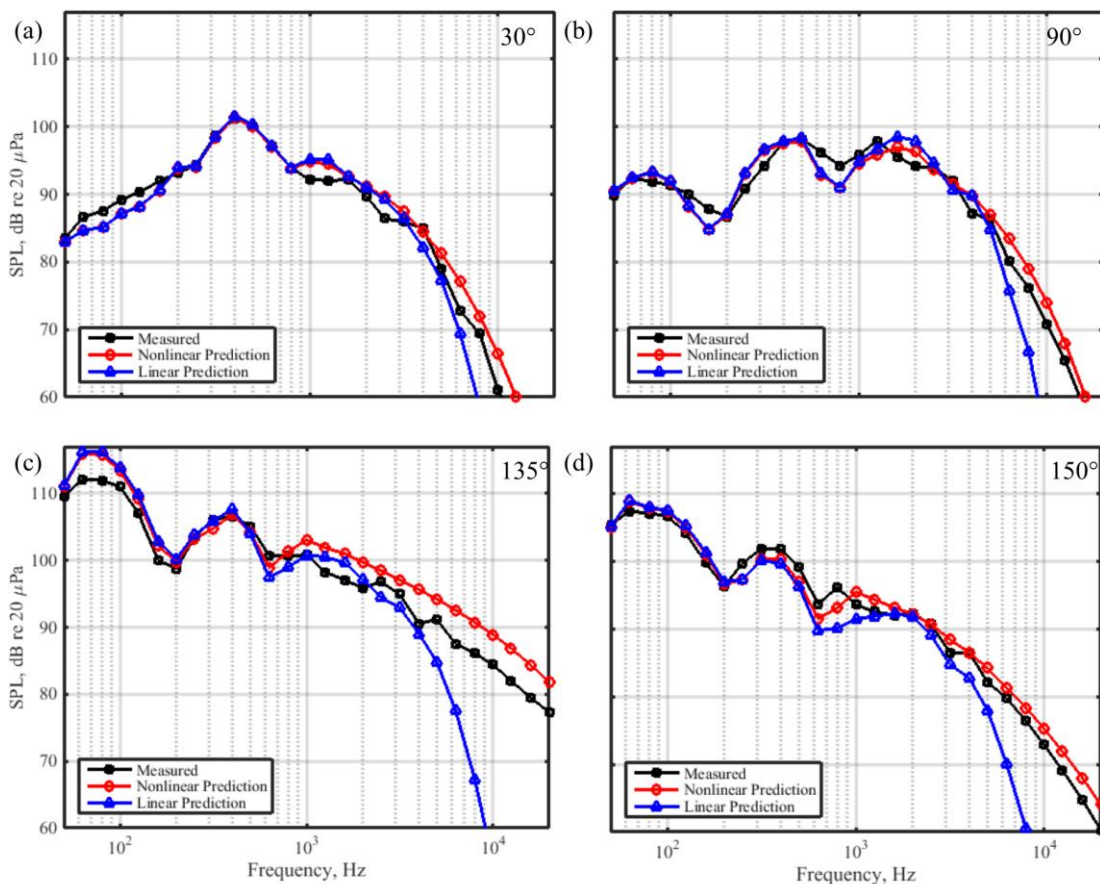


Figure 12. OTO spectra at 305 m compared with linear and nonlinear predictions for 130% ETR. Waveforms measured at $r = 76.2$ m are propagated to $r = 305$ m using both linear (blue) and a nonlinear (red) propagation algorithms. The resulting OTO spectra are compared with the spectra at 305 m (black) at (a) 30° , (b) 90° , (c) 135° , and (d) 150° .

V. Conclusions

Recent measurements have allowed a comparison of nonlinear propagation effects for full-scale military aircraft over a greater range of distances, angles, and operating conditions than previously reported. Evidence of nonlinear propagation can be seen in the time domain, evidenced by steepening waveforms, and in the frequency domain, where it is seen as high-frequency levels when linear absorption predicts losses of more than 100 dB. The presence of nonlinear effects is confirmed through a spectral comparison of calculated spectra with predictions made using linear and nonlinear propagation algorithms. The nonlinear propagation more closely aligns with the calculated spectra and show significant gains over the linear predictions at high frequencies, even to some extent in the forward direction.

Acknowledgments

The authors would like to gratefully acknowledge funding for the measurements, provided through the F-35 Program Office and Air Force Research Laboratory. B.O. Reichman was funded through by an appointment to the Student Research Participation Program at the U.S. Air Force Research Laboratory, 711th Human Performance Wing, Human Effectiveness Directorate, Warfighter Interface Division, Battlespace Acoustics Branch administered by the Oak Ridge Institute for Science and Education through an interagency agreement between the U.S. Department of Energy and USAFRL.

References

- ¹ Gurbatov, S. N. and Rudenko, O. V, "Statistical phenomena," in *Nonlinear Acoustics*, edited by M. F. Hamilton and D. T. Blackstock (Academic, San Diego, 1998), Chap. 13, pp. 377–398.
- ² Gee, K. L., Atchley, A. A., Falco, L. E., Shepherd, M. R., Ukeiley, L. S., Jansen, B. J., and Seiner, J. M., "Bicoherence Analysis of Model-Scale Jet Noise," *Journal of the Acoustical Society of America*, Vol. 128, No. 5, 2010, pp. EL211-EL216.
- ³ Petitjean, B. P., Viswanathan, K., and McLaughlin, D. K., "Acoustic Pressure Waveforms Measured in High Speed Jet Noise Experiencing Nonlinear Propagation," *International Journal of Aeroacoustics* **5**, No. 2, 2006, 193-215.
- ⁴ Gee, K. L., Sparrow, V. W., James, M. M., Downing, J. M., Hobbs, C. M., Gabrielson, T. B., and Atchley, A. A., "Measurement and Prediction of Noise Propagation from a High-power Jet Aircraft," *AIAA Journal* Vol. 45, No. 12, 2007, pp. 3003-3006.
- ⁵ Gee, K. L., Sparrow, V. W., James, M. M., Downing, J. M., Hobbs, C. M., Gabrielson, T. B., and Atchley, A. A., "The Role of Nonlinear Effects in the Propagation of Noise from High-power Jet Aircraft," *Journal of the Acoustical Society of America*, Vol. 123, 2008, pp. 4082-4093.
- ⁶ McNerny, S. A., Gee, K. L. Dowling, J. M., and James, M. M., "Acoustical nonlinearities in aircraft flyover data," *AIAA Paper 2007-3654*, May 2007.
- ⁷ McNerny, S. A., Downing, M., Hobbs, C., and Hannon, M., "Metrics that Characterize Nonlinearity in Jet Noise," *Innovations in Nonlinear Acoustics (ISNA 17)*, AIP Conference Proceedings Vol. 838, 2006, pp. 560-563.
- ⁸ Morfey, C.L., and Howell, G.P., "Nonlinear propagation of aircraft noise in the atmosphere," *AIAA J.* **19**, 986–992 (1981).
- ⁹ Baars, W. J. and Tinney, C. E., "Quantifying Crackle-inducing Acoustic Shock-Structures emitted by a Fully-Expanded Mach 3 Jet," *AIAA paper 2013-2081*, May 2013.
- ¹⁰ Baars, W. J., Tinney, C. E., and Wochner, M. S., "Nonlinear Noise Propagation from a Fully Expanded Mach 3 Jet," *AIAA Paper 2012-1177*, Jan. 2012.
- ¹¹ Pectorius, F. M. and Blackstock, D. T. "Propagation of Finite-Amplitude Noise", *Finite-amplitude wave effects in fluids: Proceedings of the 1973 Symposium*, edited by L. Bjorno, IPC Business Press Ltd, Surrey, England, 1973, pp. 24-29.
- ¹² R. O. Cleveland, J. P. Chambers, H. E. Bass, R. Raspet, D. T. Blackstock, and M. F. Hamilton, "Comparison of computer codes for the propagation of sonic boom waveforms through isothermal atmospheres," *Journal of the Acoustical Society of America*. **100**(5), 3017-3027 (1996).
- ¹³ M. O. Anderson, "The propagation of a spherical N wave in an absorbing medium and its diffraction by a circular aperture," Masters thesis, Applied Research Laboratories, The University of Texas at Austin, 1974.
- ¹⁴ H. E. Bass, R. Raspet, J. P. Chambers, and M. Kelly, "Modification of sonic boom wave forms during propagation from the source to the ground," *Journal of the Acoustical Society of America* **111**(1), 481-486 (2002).
- ¹⁵ H. H. Brouwer, "Numerical Simulation of Nonlinear Jet Noise Propagation," *AIAA Paper No. 2005-3088* (2005).
- ¹⁶ Blackstock, D. T., "Nonlinear propagation distortion of jet noise," *Proceedings of the Third Interagency Symposium on University Research in Transportation Noise*, edited by G. Banerian and P. Kickinson, Univ. of Utah, Salt Lake City, UT, 1975, pp. 389-397
- ¹⁷ Brouwer, H. H., "Numerical simulation of nonlinear jet noise propagation," *AIAA Paper No. 2005-3088*, May 2005.
- ¹⁸ Saxena, S., Morris, P. J., Viswanathan, K., "Algorithm for the nonlinear propagation of broadband jet noise,"
- ¹⁹ Gee, K. L., Downing, J. M., James, M. M., McKinley, R. C., McKinley, R. L., Neilsen, T. B., and Wall, A. T., "Nonlinear evolution of noise from a military jet aircraft during ground run-up," *AIAA Paper 2012-2258* (2012).
- ²⁰ Methods for the Measurement of Noise Emissions from High Performance Military Jet Aircraft, ANSI S12.75-2012, *AIAA Journal* Vol. 47, No. 1, January 2009, pp. 186-194
- ²¹ James, M.M., Salton, A.R., Downing, J.M., Gee, K.L., Neilsen, T.B., Reichman, B.O., McKinley, R.L., Wall, A.T., and Gallagher, H.L., "Acoustic Emissions from F-35A and F-35B during ground run-up," *Proceedings of the 21st AIAA/CEAS Aeroacoustics Conference*, (Submitted for publication 2015)
- ²² Fievet, R., Tinney, C.E., Baars, W. J., and Hamilton, M. F., "Acoustic waveforms produced by a laboratory scale supersonic jet," *AIAA Paper 2014-2906*
- ²³ ANSI, "Calculation of the Absorption of Sound by the Atmosphere," ANSI/ASA S1.26-1995 (R2009).
- ²⁴ Blackstock, D. T., Hamilton, M. F., and Pierce, A. D., "Progressive waves in lossless and lossy fluids," in *Nonlinear Acoustics* (Acoustical Society of America, Melville, NY, 2008), Chap. 4, pp. 65–150.
- ²⁵ Pierce, A. D. "Acoustics: An Introduction to Its Physical Principles and Applications" McGraw-Hill Book Company. *New York* (1981).

²⁶ Gurbatov, S. N., Demin, I. Y., Cherepennikov, V. V., and Enflo, B. O., "Behavior of intense acoustic noise at large distances," *Akusticheski Zhurnal* 53(1), pp. 55-72 (2007).

²⁷ Embleton, T. F. W., Piercy, J. E., and Daigle, G. A., "Effective flow resistivity of ground surfaces determined by acoustical measurements," *Journal of the Acoustical Society of America* 74(4), 1239-1244 (1983)

²⁸ Daigle, G. A., "Effects of atmospheric turbulence on the interference of sound waves above a finite impedance boundary," *Journal of the Acoustical Society of America* 65(1) (1979).

²⁹ Gee, K. L., Neilsen, T. B., James, M. M., "Including source correlation and atmospheric turbulence in a ground reflection model for rocket noise," *Proceedings of Meetings on Acoustics* 22, 2014